



Redox-responsive polyanhydride micelles for cancer therapy

Jie Wang^{a,1}, Guang Yang^{a,1}, Xing Guo^a, Zhaomin Tang^a, Zhendong Zhong^b, Shaobing Zhou^{a,*}



^a Key Laboratory of Advanced Technologies of Material, Ministry of Education, School of Materials Science and Engineering, Southwest Jiaotong University, Chengdu 610031, China

^b Sichuan Academy of Medical Sciences & Sichuan Provincial People's Hospital, Chengdu 610212, China

ARTICLE INFO

Article history:

Received 10 October 2013

Accepted 13 December 2013

Available online 3 January 2014

Keywords:

Micelle
Redox-responsive
Nanocarrier
Drug delivery
Cancer therapy

ABSTRACT

Biodegradable polyanhydrides possess unique features like those that they can predominantly undergo surface erosion, and the payloads can be released by a steady speed. However, there is little work that has been published to describe the polyanhydride micelles with redox-responsiveness as a nanocarrier for drug delivery. In this study, we develop one type of new amphiphilic polyanhydride copolymer containing disulfide bonds between the hydrophilic and hydrophobic segments. The copolymer can self-assemble into stable micelles with well-defined core–shell structure and a uniform size distribution with an average diameter of 69 nm. The disassembly behaviors of the micelles triggered by glutathione are evaluated from the changes of the micellar size, morphology and molecular weight. An approximate zero-order *in vitro* drug release mode with a fast speed can be achieved in a reducing and acid environment similar with that of tumor cells. *In vitro* cytotoxicity analysis demonstrate that the Cur-loaded micelles are of great efficiency in inhibiting the growth of cancer cells due to the rapidly intracellular delivery of therapeutic agent. Both the qualitative and quantitative results of the antitumor activity in 4T1 tumor-bearing BALB/c mice reveal that the redox-responsive micelles have a more significant therapeutic effect to artificial solid tumor compared to the redox-insensitive micelles. This study provides a new insight into the biomedical application of polyanhydrides in drug delivery.

© 2013 Elsevier Ltd. All rights reserved.

1. Introduction

Nanocarriers have shown tremendous promise in drug and gene delivery [1,2], since they have an ability of delivering their cargos preferentially into cancer tissues or targeted location, and in turn significantly enhance the therapeutic efficacy or transfection efficacy while substantially reducing side effects [3]. Among these nanoscaled drug delivery systems, polymeric micelles with distinct core/shell architecture self-assembled from amphiphilic copolymers have been extensively explored [4–8]. They present exceptional advantages as nanocarriers, including relatively high stability due to low critical micelle concentration (CMC), an improved solubility of poorly water soluble drugs, and prolonged blood circulation owing to their high water solubility [9–12].

In the micelle systems, the hydrophobic segments of amphiphilic copolymers mostly studied are aliphatic polyesters, such as

poly(ϵ -caprolactone) (PCL), poly(D,L-lactide) (PLA), and the hydrophilic segments are generally polyether, such as polyethylene glycol (PEG) [13,14]. Hydrophobic polyanhydrides are the most suitable candidate as a vesicle in drug delivery system due to their unique features like those that they can predominantly undergo surface erosion, and the drug can be released by a steady speed from the polymer matrix [15,16]. However, nowadays they are seldom employed to act as the hydrophobic segments of amphiphilic copolymers due to the worry of the fast degradation of polyanhydrides and subsequent instability of their nanoparticles. Nevertheless, our previous work demonstrated that the polyether-polyanhydride copolymer composed of methoxypolyethylene glycols (mPEG), 1,3-bis(carboxyphenoxy) propane (CPP) and sebacic acid (SA) could self-assemble into micelles with good stability [17,18]. Furthermore, in most cases of cancer therapy using nanocarriers, the payloads of therapeutic agents need to be released quickly into cancer cells so as to efficiently induce death of various cancer cells [19,20], and this process generally takes a short period of time from several hours to several days. It is still a challenging task for the nanoparticle-based drug delivery system that can be fast degraded for nanocarriers or be rapidly disassembled for this

* Corresponding author. Tel.: +86 28 87634068; fax: +86 28 87634649.

E-mail addresses: shaobingzhou@hotmail.com, shaobingzhou@swjtu.edu.cn (S. Zhou).

¹ These authors contributed equally to this work.

system in response to environmental stimuli after these nanoparticles are endocytosed into cancer cells.

Recently, various stimuli-responsive (e.g. temperature [21], pH [14], redox [13,22–24].) polymeric micelles have been highly concerned. Among all applied stimuli, redox potential is a potent stimuli due to the difference in glutathione (GSH) concentration existing between the reducing intracellular space (approximately 2–10 mM) and mildly oxidizing in extracellular space (approximately 2–20 μ M) [25,26]. Redox-sensitive polymers usually connect with characteristic disulfide linkages or diselenide groups which can maintain adequate stability in the circulation and extracellular milieu and tend to rapid cleavage under the reducing intracellular space [27–30].

In this study, we developed a new redox-responsive drug delivery system based on amphiphilic PEG-based ether-anhydride copolymer (mPEG-ss-CPP-SA) containing disulfide bonds between mPEG and CPP-SA segments. It can self-assemble into micelles in aqueous solution and the reduction-triggered disassembly behaviors were systematically investigated with GSH. Curcumin (Cur), a lipophilic polyphenol drug, were loaded into micelles by physical mixing method. In comparison to the redox-insensitive micelles, the intracellular drug release, cell apoptosis and cell cycle induced by the Cur-loaded micelles, antitumor effect both *in vitro* and *in vivo* and histological assessment of the redox-responsive mPEG-ss-CPP-SA micelles were systematically evaluated after being applied to the BALB/c mice bearing 4T1 tumor model.

2. Materials and methods

2.1. Materials

Monomethyl poly (ethylene glycol) (mPEG, $M_w = 2.0$ kDa) was purchased from Sigma–Aldrich (USA). Curcumin (Cur, 95%) was purchased from Chengdu laboone Company (Chengdu, China). Glutathione (GSH), 3, 3'-dithiodipropionic acid (DTDP) were purchased from Adamas-beta. Pyrene, 1, 3'-dibromopropane, *p*-hydroxybenzoic acid and sebacic acid (SA) were obtained from Chengdu KeLong Chemical Reagent Company (Chengdu, China). Cell Cycle and Annexin V-FITC Apoptosis Detection Kits were purchased from KeyGEN Biotech (Nanjing, China) and used as received. All other chemicals were of analytical grade and were used without further purification.

2.2. Cell lines and culture conditions

The human cervical cancer cell line HeLa, osteoblasts (OB) cells and murine breast cancer cells 4T1 were purchased from Sichuan University (Chengdu, China). Cells were cultured in RPMI 1640 supplemented with 10% newborn calf serum (NCS, Gibco, USA) at 37 °C and 5% CO₂ under fully humidified conditions. All experiments were performed on cells in the exponential growth phase.

2.3. Animals

Male BALB/c mice (20 \pm 2 g) used for *in vivo* antitumor tests were purchased from Experimental Animal Center of Sichuan University. Animals were provided with standard laboratory chow and tap water *ad libitum*. All animal procedures were performed according to the protocol approved by the Institutional Animal Care and Treatment Committee of Sichuan University.

2.4. Synthesis procedures

2.4.1. Synthesis of prepolymers

1, 3-Bis-(carboxyphenoxy) propane (CPP) was prepared according to our earlier studies with a yield of 40–50% [17,18]. As shown in Scheme S1 in Support Information (SI), the dicarboxylic acid monomers are converted to the mixed anhydride of acetic acid by refluxing in excess acetic anhydride. Briefly, preweighed dicarboxylic acid monomers (SA, CPP, DTDP) were respectively refluxed in excess acetic anhydride (w/v = 1:10) under the protection of argon, followed by filtration and concentrated under vacuum at 60 °C to remove the unreacted diacid and acetic anhydride residues. After dried under vacuum, the prepolymers were obtained with yields ranging from 56% to 63%.

2.4.2. Synthesis of copolymers

The final mPEG-ss-CPP-SA copolymer was synthesized via classical melt-condensation polymerization (Scheme S1). In brief, mPEG, DTDP prepolymer, SA prepolymer and CPP prepolymer were mixed in a weight feed ratio of 40:5:35:20 in a three-neck round-bottom flask. The flask was immersed in an oil bath at 180 °C, after the prepolymers were melted, high vacuum was applied. At the end of the

reaction, the mixtures were allowed to cool completely and dissolved in dichloromethane. Finally the copolymer was precipitated using anhydrous ether and dried under vacuum with yields ranging from 62% to 70%. At the same time, the redox-insensitive copolymer, mPEG-CPP-SA, was also synthesized with the same procedure as described above. All products obtained were stored at –20 °C for further use.

2.5. Micelle formation

The blank micelles of mPEG-ss-CPP-SA and mPEG-CPP-SA were prepared by dropwise addition of 5.0 mL block copolymer solution in THF to 10.0 mL deionized water under stirring, followed by the removal of THF at room temperature.

The hydrophobic anticancer drug Cur was used as a model for fabricating Cur-loaded mPEG-ss-CPP-SA (Cur-ssM) and mPEG-CPP-SA micelles (Cur-M). The procedure is almost similar with that of blank micelles. The differences are that Cur was dissolved in THF together with copolymer, and the final micelle solution was transferred into dialysis bag (MWCO 1000) against deionized water for 36 h to remove the free Cur. Finally, the samples were lyophilized and stored at –20 °C for future use.

2.6. Characterization

Fourier transform infrared spectrometer (FT-IR) spectra were recorded on a Nicolet 5700 spectrometer by KBr sample holder method. Nuclear magnetic resonance (¹H NMR) spectra were obtained on a Bruker AM 300 apparatus with CDCl₃ or D₂O as solvents and TMS as an internal reference. The number-average molecular weight (M_n), weight-average molecular weight (M_w), and M_w/M_n were measured by gel permeation chromatography (GPC). For GPC (Waters 1515, USA) measurement, dimethylformamide (DMF)/LiBr was used as the eluent at a flow rate of 1 mL/min at 40 °C, and polymethyl methacrylate (PMMA) was used as reference. All samples with concentration of 1.00 mg/mL were filtered with a 0.22 μ m syringe filter before measurement. Dynamic light scattering (DLS) measurements were performed in aqueous solution using a Malvern Zetasizer Nano-ZS90 apparatus. Transmission electron microscopy (TEM) studies were performed with a JEOL 2100F instrument (JEOL Ltd., Japan) operated at 200 kV. Atomic force microscopy (AFM) (CSPM5000, Beijing, China) was employed with tapping-mode to further observe the morphology. Critical micelle concentration (CMC) was determined with a Fluoromax spectrometer (F-7000, Hitachi, Japan) at room temperature.

Drug loading content (LC) and encapsulation efficiency (EE) were measured with UV–vis spectrophotometer (UV-2550, Shimadzu, Japan). The amount of released drug in the incubation medium was quantified by high performance liquid chromatography (HPLC, Agilent 1260 Infinity) with UV detector.

2.7. Reduction-triggered disassembly behaviors of mPEG-ss-CPP-SA micelles

To evaluate the reduction-triggered disassembly behaviors of mPEG-ss-CPP-SA micelles, the size change of micelles (3 mL, 1 mg/mL) in response to different GSH concentration (20 μ M, 0.5 mM, 10 mM) in PBS buffer (pH = 7.4, 0.01 M) was investigated by DLS measurement. The excitation spectra of the solutions with 10 mM GSH were recorded with a Fluoromax spectrometer. The morphology change of micelle before and after adding 10 mM GSH for 4 h was measured by TEM.

2.8. Reduction-triggered drug release *in vitro*

The *in vitro* release kinetics of Cur from micelles were investigated in four different media all containing Tween-80 (0.5% w/w), i.e. phosphate buffer saline (PBS, 0.01 M, pH 7.4) with or without 10 mM GSH and acetate buffer saline (ABS, 0.2 M, pH 5.0) with or without 10 mM GSH. The freeze-dried sample was diluted to 1 mg/mL and 1.0 mL of this solution was transferred into a dialysis bag (MWCO 1000). It was immersed into a tube containing 30 mL of incubation media in a shaking bed at 100 rpm and 37 °C. The amount of released drug in the incubation medium was quantified by HPLC.

2.9. *In vitro* biocompatibility evaluation

2.9.1. Cytotoxicity assay

The cytotoxicity studies were carried out to investigate whether the copolymers affect cell proliferation of the HeLa cells and OB cells based on Alamar blue assay. Cells were seeded into 48-well plate at a density of 1×10^4 cells/well, and the blank micelles at the concentrations ranging from 40 μ g/mL to 800 μ g/mL were added to incubate for future 24 h. A sample of 200 μ L of Alamar blue solution was pipetted into a 96-well plate after 4 h incubation and the absorbances were read in an automated microplate spectrophotometer (ELX800 Biotek, USA) at 570 nm (excitation)/600 nm (emission). The cell morphology was observed with an inverted phase contrast microscope (Nikon Eclipse TS100, Japan).

2.9.2. Hemocompatibility test

The hemolysis properties of both the blank micelle and drug-loaded micelle were examined by spectrophotometry with the similar procedure described by Guo et al. [14]. The absorbance of the samples was measured in an automated microplate spectrophotometer at 540 nm and the hemolysis ratio (HR) was calculated using Formula (1):

$$\text{HR}(\%) = \frac{A_{\text{sample}} - A_{\text{negative control}}}{A_{\text{positive control}} - A_{\text{negative control}}} \times 100 \quad (1)$$

wherein *A* means the absorbance.

2.10. *In vitro* antitumor activity assay

The antitumor activity of Cur-loaded micelles (Cur-ssM, Cur-M) and free Cur was studied with the HeLa cells with Alamar blue assay. Briefly, HeLa cells were plated in a 48-well plate at a density of 1×10^4 cells/well. After an overnight attachment period, the Cur-loaded micelles with Cur dosages varying from 0.1 $\mu\text{g}/\text{mL}$ to 50 $\mu\text{g}/\text{mL}$ were added to incubate for future 48 h. The cell viabilities were determined as the cytotoxicity studies described above.

2.11. Intracellular drug release

The cellular uptake and intracellular release behaviors of the Cur-loaded micelles were investigated by fluorescence microscopy (FM), confocal laser scanning microscopy (CLSM) and flow cytometry (FCM) against HeLa cells. After different incubation time intervals, the cells were then fixed with 2.5% glutaraldehyde for 50 min and cell nuclei were stained with 4, 6-diamidino-2-phenylindole (DAPI, blue) for 7 min. The fluorescence images were taken using an inverted fluorescence microscope (Olympus, CKX41) and CLSM (FV1000, Olympus, Japan). For flow cytometric analysis, after presetting incubation time, the cells were washed three times with PBS, followed by trypsin and centrifugation at 2000 rpm for 3 min to harvest the cells, then ten thousands cells were gated and analyzed for fluorescent intensity per cells with the flow cytometer (BD Accuri C6, USA).

2.12. Cell apoptosis and cell cycle assay

To confirm the therapeutic effect of the three Cur formulations, we performed the cell apoptosis and cell cycle assays by FCM. First, HeLa cells were seeded in 6-well plates at a density of 1×10^5 cells/well and incubated at 37 °C for 24 h. Then the cells were treated with free Cur, Cur-M and Cur-ssM containing 20 $\mu\text{g}/\text{mL}$ equivalent Cur to incubate for future 24 h. The rate of apoptosis was measured by using Annexin V-FITC Apoptosis Detection Kit in accordance with the manufacturer's protocol.

2.13. *In vivo* tumor growth and biodistribution studies

To establish tumor models, 1×10^6 4T1 cells in 100 μL medium were inoculated subcutaneously at the lower right flank of the BALB/c mice. About 10 days post inoculation, tumors in the mice were detachable and reached a volume around 50 mm^3 (designated as the day 0). Mice were randomly divided into five groups ($n = 7$) and received intravenous administration of saline, blank micelle, free Cur, Cur-M and Cur-ssM at 10 mg/kg equivalent Cur, respectively. The treatments were performed every two days and lasted for 4 times. Mice weight and tumor size were also monitored every two days after the first treatment. The tumor size was measured using a vernier caliper across its longest (a) and shortest (b) diameters and calculated with the equation $\text{volume} = ab^2/2$. For biodistribution evaluation, tumor-bearing mice were randomized into three groups ($n = 3$) and injected intravenously with 100 μL saline at a dosage of 10 mg Cur/kg body weight of free Cur, Cur-M and Cur-ssM (10 mg/kg), respectively. At indicated times, the mice were sacrificed by cervical dislocation. Tissue samples (i.e. heart, liver, spleen, lung, kidney and tumor) were collected and washed with saline, blotted with filter paper, weighed, then placed in 1 mL saline and homogenized, respectively. Then the homogenized samples were extracted with ethyl acetate and vortexed for 5 min and centrifugated for 5 min at 3500 r/min, respectively. The supernatants were collected and evaporated to dryness. The obtained dry residues were then dissolved in methanol and filtered through a 0.22 μm syringe filter. 20 μL of filtrate was collected for HPLC analysis. Tissue distribution was expressed as the amount of Cur per gram of the tissues.

2.14. Histological assessment

At day 21, portions of mice were sacrificed and their tumor tissues were collected in 4% formaldehyde and embedded in paraffin blocks after dehydrating with gradient ethanol. Then tissue sections of 5 μm were dewaxed and stained with hematoxylin and eosin (H&E) or detected with the In Situ Cell Death Detection Kit, POD (Roche Diagnostics GmbH, Mannheim, Germany) for microscopic observation. The mean optical density (OD) values were measured from three pictures of each sample with Image-Pro Plus 6.0 software and the results were the average data with standard deviations.

2.15. Statistical analysis

Data were expressed as the mean value \pm standard deviation. Single factorial analysis of variance (ANOVA) was performed to determine statistical significance of the data.

3. Results and discussion

3.1. Characterization of mPEG-ss-CPP-SA copolymers

The composition and structure of redox-sensitive mPEG-ss-CPP-SA copolymer were confirmed by FT-IR, ^1H NMR, and GPC. In Fig. S1A in SI, the FT-IR spectra display some clear signals attributable to the characteristic absorption bands of anhydride carbonyl (1810 cm^{-1} , 1739 cm^{-1}), ether bond (1110 cm^{-1} , 1084 cm^{-1}) and methylene (2921 cm^{-1}), respectively. With further characterization of ^1H NMR (Fig. S1B), we can find that in mPEG-ss-CPP-SA spectrum two new peaks at 2.89 and 2.86 ppm occurred in contrast to the spectrum of mPEG-CPP-SA, suggesting that the successful introduction of disulfide bond into this copolymer. The other peaks of both copolymers are consistent with previous reports [17,18]. The actual ratio of mPEG, disulfide bonds, CPP and SA components calculated from ^1H NMR is 30.3:3.9:22.2:43.6, which is almost in agreement with feed ratio. The molecular weight and its distribution of the copolymers were further verified by GPC (Fig. S1C), and the analysis results are summarized in Table S1 in SI. We can find that both the copolymers have a narrow distribution with polydispersity of 1.3–1.07, also indicating that both polyanhydride copolymers possess a defined chemical structure. The number-average molecular weight (M_n) of mPEG-CPP-SA and mPEG-ss-CPP-SA is 11,200 and 13,100 g/mol, respectively.

3.2. Characterization of micelles

A series of measurements were employed to verify the formation of the stable micelles self-assembled from amphiphilic mPEG-CPP-SA and mPEG-ss-CPP-SA copolymers. Firstly, the CMC values of micelles derived from the plot of I_{339}/I_{333} ratio vs copolymer concentration using pyrene as a probe were shown in Fig. S2 in SI. The low CMC values (2.04 mg/L and 3.01 mg/L) can guarantee the micelle to retain a good stabilization under very dilute aqueous milieu such as blood and body fluids before reaching the targeting site. Secondly, another evidence for the micelle formation was performed by the ^1H NMR in D_2O as shown in Fig. 1A. The signals of the hydrogen atoms of methylene group in mPEG units and the solvent peak of D_2O were detected at 3.55 ppm and 4.64 ppm and the signals of the hydrogen atoms in the polyanhydride segment almost disappeared in D_2O as compared with that of the copolymer in CDCl_3 shown in Fig. S1B, which demonstrated that the copolymer formed a well-defined micellar structure with hydrophobic inner core (polyanhydride segments) and a hydrophilic outer shell (mPEG segments). Thirdly, DLS measurement further revealed that the mPEG-ss-CPP-SA micelles had a uniform size distribution with an average diameter of 69 nm (Fig. 1B). The small size of particles is most suitable for nanocarriers passively accumulating in tumor tissues via the enhanced penetration and retention (EPR) effect [1,31]. Finally, both the TEM and AFM images in Fig. 1C, D showed that the mPEG-ss-CPP-SA micelles are relatively uniform spherical in shape and have a smaller diameter in size compared with that determined by DLS, which is attributed to the fact that the dehydration of the micelles during sample preparation can cause the shrinkage of the mPEG shell.

3.3. Disassembly behaviors of micelles triggered by glutathione (GSH)

To demonstrate the disassembly behaviors of mPEG-ss-CPP-SA micelles triggered by GSH, a comprehensive characterization was conducted with a variety of ways. First, we examined the micellar size changes triggered by GSH with various concentrations by DLS. As shown in Fig. 2A, there was no significant change in size within

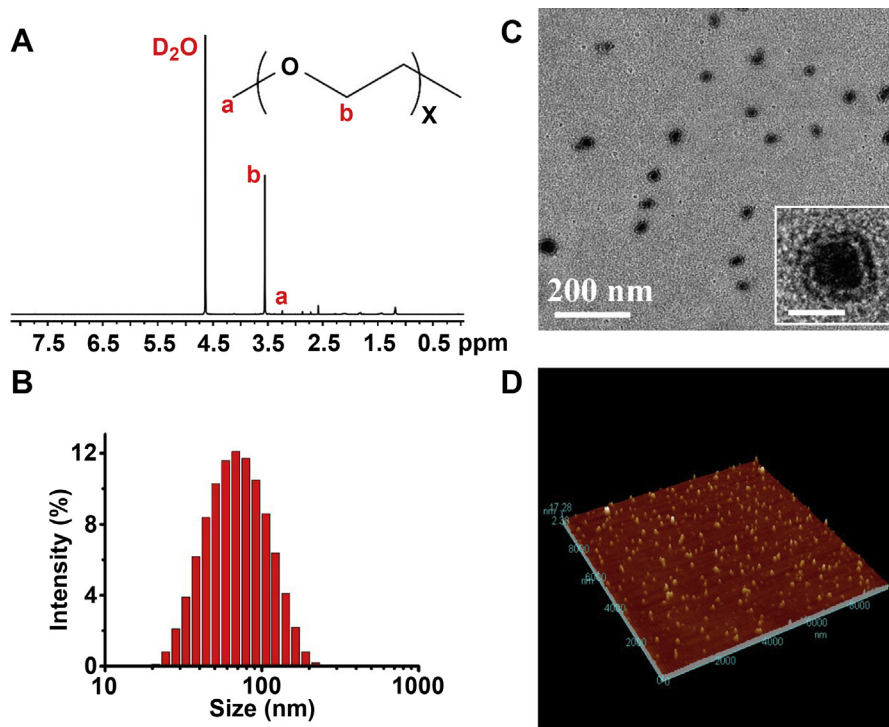


Fig. 1. ¹H NMR spectrum of mPEG-ss-CPP-SA copolymer in D₂O (A), Particle size distribution of mPEG-ss-CPP-SA micelles determined by DLS (B), and The typical morphology of mPEG-ss-CPP-SA micelles detected by TEM (C) and AFM (D). The inserted scale bar is 50 nm.

4 h under the concentration of 20 μ M GSH which is the same with the concentration of GSH in normal tissues in the body such as blood, almost an astomotic with that in the absence of GSH. In contrast, the micellar size increased from 69 nm to 175 nm, and the size distribution shifted from a unimodal peak to multimodal peaks after adding 10 mM GSH during 4 h (Fig. 2B), indicating the rapid disassembly of these micelles triggered by the mimicking reducing environment of tumor cells [32].

To further demonstrate the destruction of these micelles, fluorescence excitation spectra of the mPEG-ss-CPP-SA micellar solution were recorded by fluorescence spectrometer with a pyrene concentration of 2.0×10^{-6} M and the I_{339}/I_{333} ratio at different time intervals after addition of 10 mM GSH (Fig. 2C, D). It could be clearly observed that I_{339}/I_{333} abruptly decreased at a certain concentration after 10 mM GSH added. This indicated that the surrounding environment of pyrene was changed from the hydrophobic micelle core to the polar aqueous solution, most probably due to the redox-sensitive cleavage of the disulfide bonds of the copolymer and subsequently the disassembly of the micelles. Fig. 2E clearly illustrated the micellar morphology with irregular-shape and larger-size fragments upon exposure to 10 mM GSH for 4 h. Furthermore, from GPC analysis (Fig. 2F), we can also find that with increasing time after GSH added, the main peaks on the GPC curve moved to the small molecular weight region, also attributing to the cleavage of the disulfide bonds. In a word, the mPEG-ss-CPP-SA micelles have an ability of the redox-sensitivity and are suitable as a nanocarrier for intracellular delivery of drug in cancer therapy.

3.4. *In vitro* drug release from Cur-loaded micelles

The aqueous insolubility and instability and thereby poor bioavailability prevent Cur from effectively clinical applications [33,34]. The limitations can be significantly improved by

encapsulating Cur into polymeric micelles, and in the mPEG-ss-CPP-SA (Cur-ssM) and mPEG-CPP-SA (Cur-M) micelles, the Cur loading content and encapsulation efficiency were approximately 8% and 80%, respectively. *In vitro* Cur release behaviors of the drug-loaded micelles were performed in PBS (pH = 7.4, 0.01 M) and ABS (pH = 5.0, 0.2 M) with or without 10 mM GSH, which were used to simulate the tumor acidic and normal physiological environment, respectively. Tween-80 was selected as an emulsifier on the basis of maximum *in vitro* bioaccessibility of Cur [35]. As shown in Fig. 3A, Cur-ssM and Cur-M were considerably stable in PBS at pH 7.4 and less than 10% of Cur was released in 72 h in the absence of GSH, while with the addition of 10 mM GSH, the release percentage was significantly increased to nearly 25%. Moreover, the drug release rate was promoted significantly in ABS at pH 5.0. It is noteworthy that these redox-responsive polyanhydride micelles possess an approximately steady and sustained release, and no obvious burst release can be found in contrast to the copolymer micelles derived from PEG and aliphatic polyesters most frequently studied [14,25,32]. As it has been proposed that polyanhydrides can predominantly undergo surface erosion and erode heterogeneously at rates suitable for controlled release. Moreover, with the activation of GSH, the cleavage of the disulfide bonds occurred, and in turn the bare hydrophobic cores loaded with drug were generated (Fig. 3B). So, the drug release at a steady speed was acquired due to the fact that polyanhydride is surface eroding with a predictable degradation rate [16,36,37]. Additionally, the stability of Cur is pH-dependent and the degradation occurs faster at neutral-basic conditions [38]. Under acidic conditions, its structure can be maintained, which endows it the efficiency for the cancer treatment. Herein, we also find that the release of the Cur was faster at pH 5.0 than that at pH 7.4. This release profile is just expected in the cancer treatment since the pH value of early endosome in tumor cells is around 5–6 while the late lysosome is much more acidic compartment (pH 4–5) [39,40].

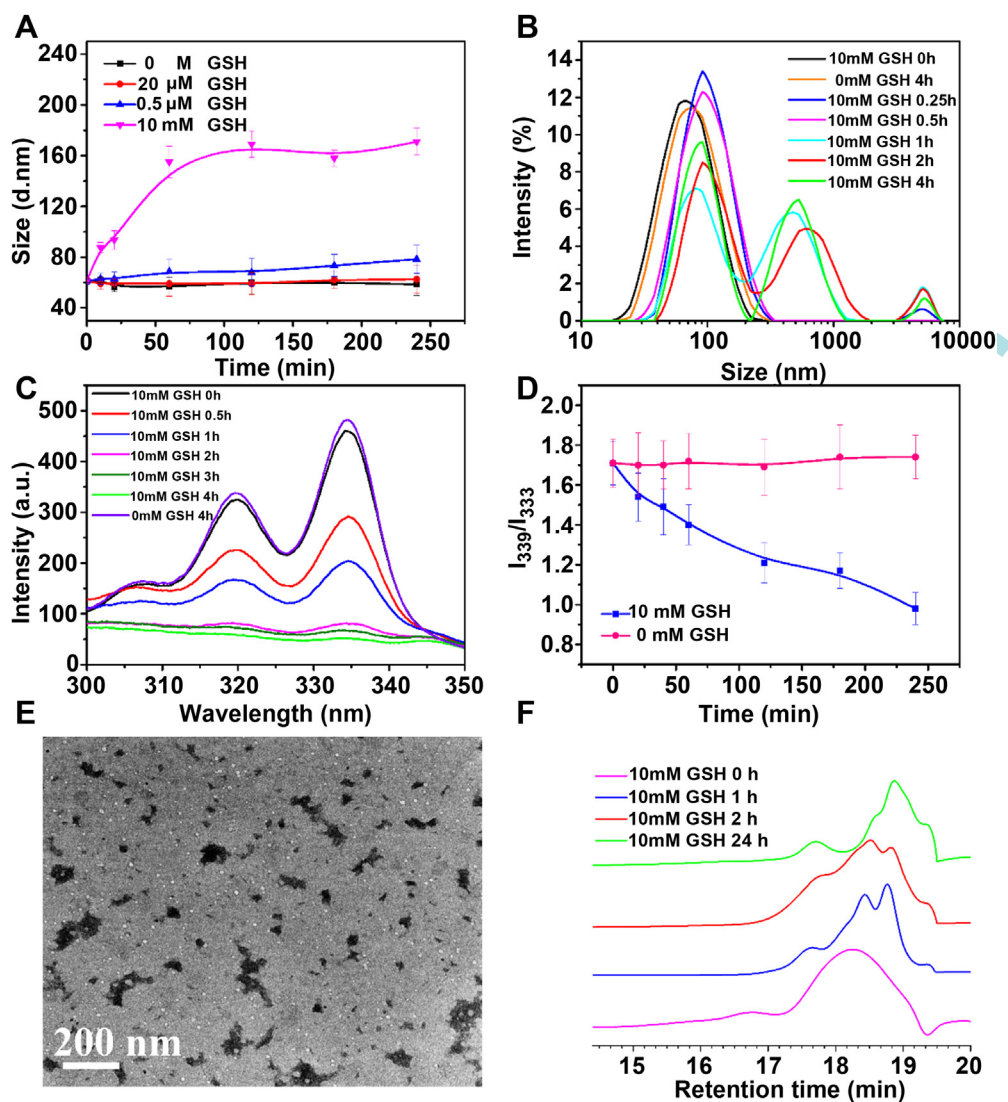


Fig. 2. The disassembly behaviors of mPEG-ss-CPP-SA micelles in response to GSH: Time-dependent changes in micellar diameter in the absence or presence of 20 μM , 0.5 mM and 20 mM GSH in PBS at pH 7.4 at 37 $^{\circ}\text{C}$ (A), Change of size distribution profiles of these micelles triggered with 10 mM GSH (B), Fluorescence excitation spectra of the micellar solution at different time intervals after addition of 10 mM GSH (C), The I_{339}/I_{333} ratio vs time upon exposure to 10 mM GSH (D), The morphological change detected by TEM after incubation with 10 mM GSH for 4 h (E) and GPC curves of mPEG-ss-CPP-SA recorded at different time intervals after addition of 10 mM GSH (F). ($n = 3$).

3.5. Biocompatibility analysis

Fig. S3A–D in SI showed the viability and representative optical microscope images of HeLa and OB cells treated with blank micelles. We can find that more than 85% of the cells remained viable, and their growth is healthy, suggesting that the copolymer is noncytotoxic. Moreover, the blank and drug-loaded micelles showed negligible hemolysis rates, even at a very high concentration of 2.0 g/L, suggesting that the micelles had excellent blood compatibility and could be suitable for *in vivo* drug delivery (Fig. S4 in SI).

3.6. *In vitro* antitumor effect

A dose-dependent manner in the tumor cell viability was observed in all cases (Fig. 3C). The IC_{50} values for the Cur-M, Cur-ssM and free Cur were found to be 15.4, 8.9 and 7.7 $\mu\text{g}/\text{mL}$, respectively. The significant difference of IC_{50} between Cur-M and Cur-ssM may be contributed to the unequal cumulative Cur release as shown in Fig. 3A. Nevertheless, the Cur-ssM exerted a

comparable cytotoxic effect on HeLa cells after incubation for 48 h in contrast to free Cur at the same dose. Besides, from the *in vitro* Cur release profile of the redox-responsive micelles (Fig. 3A), we can also speculate that Cur-ssM can exert continuous suppression effect on cancer cells with sustained Cur release compared with free drug. It is noted that in this study free Cur was dissolved with the aid of DMSO and the final concentration of DMSO in the medium was ensured at less than 0.1%, which had no effect on cell proliferation [33,41].

3.7. Intracellular release of Cur

FM was firstly employed to qualitatively observe the internalization process as a function of time in HeLa cells cultured with free Cur, Cur-M and Cur-ssM (Fig. S4–S6 in SI). We can find that the cellular uptake of the three cases showed a time-dependent increase trend during the observation time. CLSM images were used to further follow the cellular localization of Cur. After 0.5 h of incubation with free Cur, Cur-M and Cur-ssM, green fluorescence of Cur was visibly observed in cell cytoplasm and mainly in nuclei

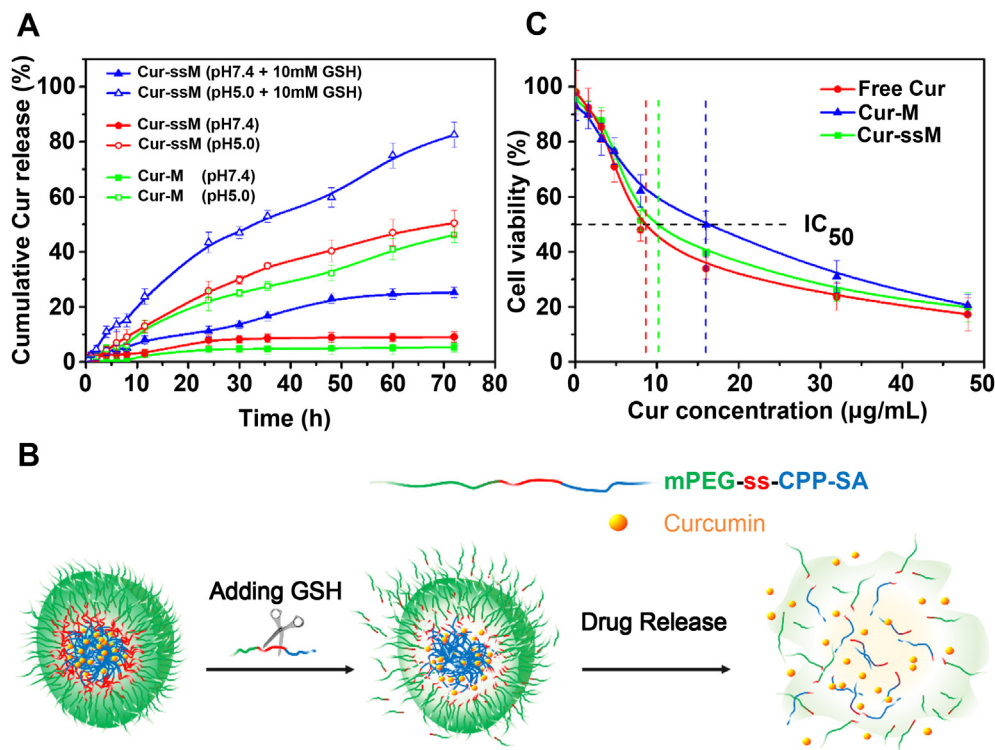


Fig. 3. *In vitro* Cur release from Cur-ssM and Cur-M micelles triggered with 10 mM GSH or without in PBS (pH 7.4) and ABS (pH 5.0) at 37 °C (A), Schematic illustration of the release mechanism of the redox-responsive micelles (B), and Cytotoxicity of HeLa cells treated by free Cur and Cur-loaded micelles as a function of Cur concentration (C). ($n = 3$).

(Fig. 4A). We can deduce that the green fluorescence located in nucleus is ascribed to the released Cur molecules rather than the drug-loaded micelles, since the nuclear pore size is much smaller than the drug-loaded micelles. When the incubation period was elongated to 3 h, the Cur fluorescence in the nuclei slightly increased for the three cases (Fig. 4B). It was noted that the cells exhibited obvious morphological changes with cell rounding, chromatin condensation and nuclear shrinkage compared with these at 0.5 h incubation, in particular for Cur-ssM group. The cellular accumulation of Cur in HeLa cells was similar between the treatments with Cur-ssM and Cur-M. However, the fluorescence intensity of cells treated with Cur-ssM was higher than that in cells treated with Cur-M according to the quantitative analysis by FCM (Fig. 4C and D), which could be attributed to the rapid release of Cur triggered by the high concentration of GSH in tumor cells. The cellular uptake of free Cur was more than that of Cur-loaded micelles at initial 0.5 h but less than those at 3 h. This may be due to the different endocytosis mechanisms of the two cases. Free Cur molecules can quickly diffuse into the cell through cell membrane, while the drug-loaded nanoparticles are mainly internalized by endocytosis [42]. The intracellular release result indicates that redox-responsive mPEG-ss-CPP-SA micelle has a capability of delivering and rapidly releasing the antitumor agents in cancer cells.

3.8. Cell apoptosis and cell cycle assay

Cur can inhibit the proliferation and survival of almost all types of tumor cells and the corresponding mechanisms about how Cur kills tumor cells are controversial [43]. To date, cell cycle arrest is one of the universally accepted mechanisms. To evaluate the impact of Cur-loaded micellar formulation on pharmacological effect, cell apoptosis and cell cycle distribution analyses induced by both the free Cur and Cur-loaded micelles were conducted, as shown in Fig. 5. From Fig. 5A, we can find that after 24 h incubation,

the total apoptotic HeLa cell populations induced by free Cur and Cur-ssM were 39.3% and 37.0%, respectively, which were slightly higher than that (25.8%) of Cur-M. Analysis of cell cycle indicated that the three Cur formulations could effectively arrest HeLa cells in the G0/G1 phase after 24 h incubation. Compared to free Cur, Cur-ssM had a relatively higher arrest proportion of cells in the G0/G1 phase but without significant differences between these groups (Fig. 5B). This may be due to the fact that free Cur diffused and accumulated directly at action sites of tumor cells while Cur-ssM showed a rapid release of Cur inside cancer cell and thereby activated apoptotic signals to induce tumor cell death. These results are consistent with the documented report that Cur is able to arrest cells in the G0/G1 phase and inhibit the proliferation of rhabdomyosarcoma cells in a p53-independent manner [44].

3.9. Biodistribution and antitumor efficiency *in vivo*

The experimental process of the *in vivo* tumor inhibition was shown in Fig. 6A. To measure the accumulated Cur in major organs and tumors at 1, 6, and 24 h after intravenous administration of free Cur, Cur-M and Cur-ssM at 10 mg/kg Cur equivalent, the tissue samples were analyzed according to the report by Song et al. [45] and the final results were gathered in Fig. 6B. After administration for 1 h, 6 h and 24 h, the accumulations of Cur-ssM and Cur-M in tumors were all significantly enhanced in comparison to free Cur. This can be attributed to two factors, one is the protection of micellar carrier with bulky hydrophilic outer shell to evade specific recognition by the reticuloendothelial system (RES) [46], the other is the well-known enhanced penetration and retention (EPR) effect in tumor tissues with tortuous and leaky vasculatures [47]. Besides the tumor tissues, the main accumulation of Cur in normal tissues was observed in lung, liver and spleen, which are the major distribution sites and target organs that are involved in the nonspecific uptake by the RES for nanomaterials [48,49].

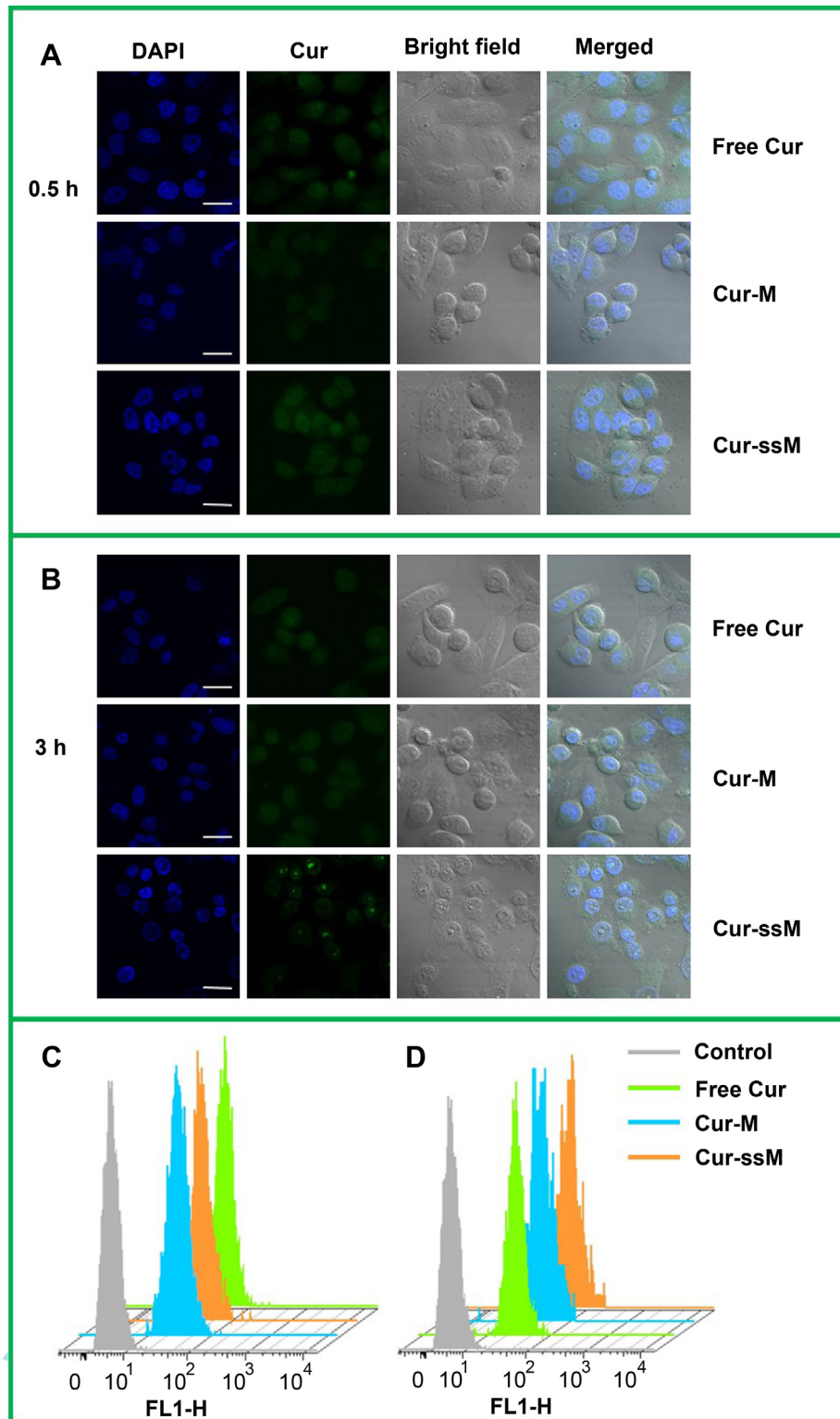


Fig. 4. Representative confocal microscopy images and flow cytometry analyses contrasting the level of cellular uptake between HeLa cells incubated with free Cur, Cur-M and Cur-ssM formulations for 0.5 h (A, C) and 3 h (B, D). (Scale bars: 50 μ m).

3.10. Antitumor efficiency *in vivo* and histological analysis

Although both the Cur-M and Cur-ssM showed no significant difference in the *in vivo* distribution, the Cur-ssM group produced the most noticeable efficiency in regressing tumor growth with 2.3 and 3.5 times higher inhibition efficiency than Cur-M and free Cur

groups (Fig. 6C). From the discussion in Figs. 3A and 4, we know that the Cur-ssM could disassemble immediately in the reducing and acid microenvironment and subsequently release the payloads rapidly, leading the cancer cells death. Free Cur could not achieve obvious antitumor effect due to its poor hydrophilicity and short half-life in blood [45,50]. The weak antitumor efficiency in Cur-M

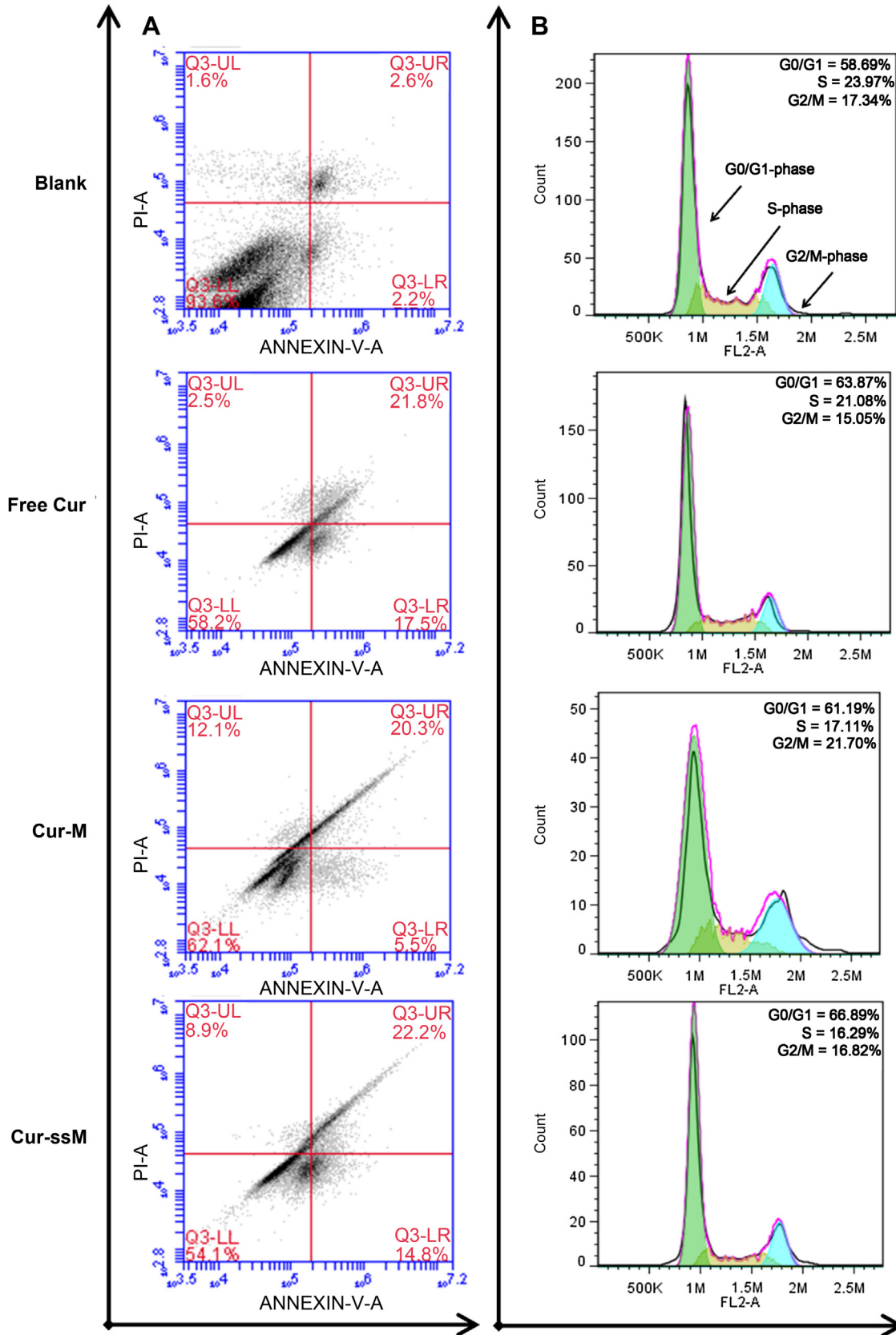


Fig. 5. Cell apoptosis (A) and cell cycle distribution (B) induced by free Cur and Cur-loaded micelles in HeLa cells. Cells were treated with an equivalent Cur dose of 15 $\mu\text{g}/\text{mL}$ after 24 h incubation and stained with annexin V-FITC and PI or incubated with RNase and PI for FACS.

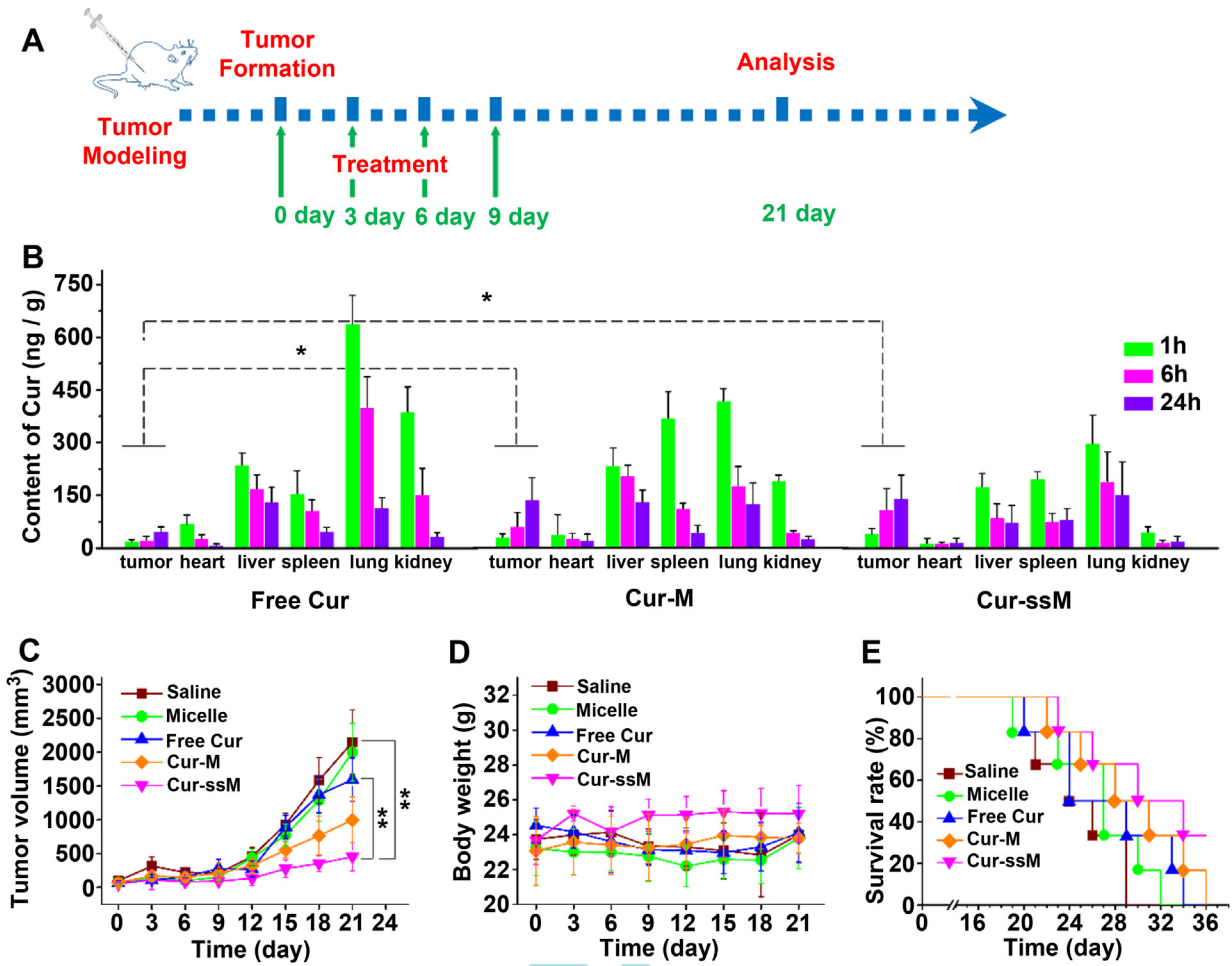


Fig. 6. *In vivo* biodistribution and therapeutic efficacy of these nanoformulations: A experimental schedule for antitumor study *in vivo* (A), Biodistribution in tissue in mice after i.v. administration of free Cur, Cur-ssM and Cur-M for different time (B), Changes of tumor volume (C), body weight (D) and survival rate (E) of tumor-bearing BABL/c mice receiving intravenous injection of saline, blank micelle and free Cur, Cur-ssM, Cur-M at a Cur dose of 10 mg/kg (* $p < 0.05$ and ** $p < 0.01$).

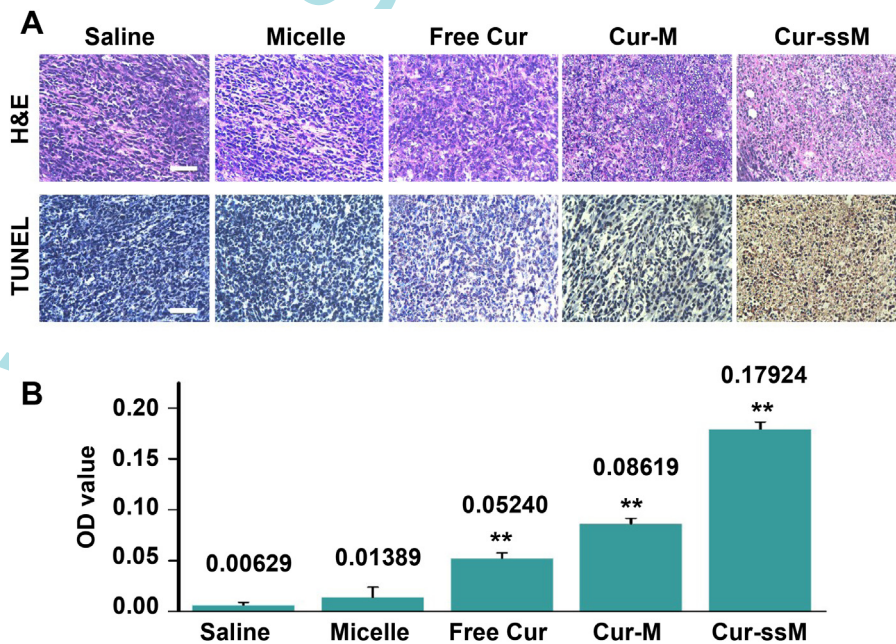


Fig. 7. H&E staining and TUNEL analysis of tumor sections at the 21st days after the first treatment (A) and the mean optical density measured with Image-Pro Plus 6.0 software based on TUNEL images (B). ** $p < 0.01$ vs. saline group. (Scale bars: 200 μ m).

group could be owing to the low Cur intracellular release from the redox-insensitive micelles as discussed in Fig. 3A. In addition, the body weight of mice in the Cur-ssM group increased obviously, in the Cur-M group almost kept no change while the other three groups decreased slightly as shown in Fig. 6D, also suggesting that the redox-responsive micelle can reduce the toxicity of therapeutic agent to normal tissues or organs. The survival rate of the mice after treatments shown in Fig. 6E also demonstrated that the therapeutic effect of Cur-ssM was remarkably better than that of Cur-M and free Cur.

To further confirm the therapeutic efficacy, histological analysis of tumor sections was performed at the 21st day after the first injection and the results were shown in Fig. 7. From the H&E staining in Fig. 7A, we can find that in comparison with saline and blank micelle groups, Cur-induced groups including free Cur, Cur-M and Cur-ssM exhibited distinct apoptosis degrees, along with cells becoming smaller, nuclei lysis, vacuoles appearing and membrane integrity destruction, especially for the Cur-ssM treated group. Apoptotic cells in dark brown were also identified by TUNEL assay (Fig. 7A). For Cur-ssM group, we can clearly observe that nuclear membrane cracked and chromatin condensed, marginalized and divided into blocks or apoptotic bodies, which is an obvious signal for the apoptosis of tumor cells as previous reports [51,52]. In biology, OD is commonly used for immunohistochemical examination. Usually the deeper the stained lesion, the larger the optical density. To quantify the apoptosis of each group, the lesions with dark brown represents the apoptotic cells in TUNEL assay images and the mean OD of these lesions was calculated with Image-Pro Plus 6.0 software and shown in Fig. 7B. The OD value (0.17924) of the Cur-ssM group is the highest and has significant difference with the other groups, especially compared to the saline group (0.00629), also indicating the excellent superiority in inducing apoptosis of cancer cells *in vivo*.

4. Conclusion

In summary, we have successfully developed one type of redox-responsive polyanhydride copolymer, and acquired stable micelles with well-defined core-shell structure by self-assembly of this copolymer. The desirable redox-sensitivity of micelles is verified by changing the concentration of the reducing agent GSH. *In vitro* release profiles demonstrate that the therapeutic agent Cur can be released from the polymer matrix at a steady and rapid speed in a reducing and acid environment. *In vitro* cytotoxicity analysis reveals that Cur loaded redox-responsive micelles are more effective in inhibiting the growth of tumor cells due to the rapid release of therapeutic agent in tumor microenvironment in contrast to redox-insensitive micelles. *In vivo* antitumor activity demonstrates that the redox-responsive micelles possess higher safety to the body and a better therapeutic effect in the induction of tumor necrosis compared with redox-insensitive micelles. Therefore, the study provides a facile strategy towards the design and engineering of the next-generation nanomedicines for cancer therapy.

Acknowledgments

This work was partially supported by National Basic Research Program of China (973 Program, 2012CB933600), National Natural Science Foundation of China (51173150, 51373138), National Key Project of Scientific and Technical Supporting Programs Funded by MSTC (2012BAI17B06), Research Fund for the Doctoral Program of Higher Education of China (20120184110029) and Fundamental Research Funds for The Central Universities (SWJTU11ZT10).

Appendix A. Supplementary data

Supplementary data related to this article can be found at <http://dx.doi.org/10.1016/j.biomaterials.2013.12.025>.

References

- [1] Peer D, Karp JM, Hong S, Farokhzad OC, Margalit R, Langer R. Nanocarriers as an emerging platform for cancer therapy. *Nat Nanotechnol* 2007;2:751–60.
- [2] Newland B, Zheng Y, Jin Y, Abu-Rub M, Cao H, Wang W, et al. Single cyclized molecule versus single branched molecule: a simple and efficient 3D “knot” polymer structure for nonviral gene delivery. *J Am Chem Soc* 2012;134:4782–9.
- [3] Farokhzad OC, Langer R. Impact of nanotechnology on drug delivery. *ACS Nano* 2009;3:16–20.
- [4] Duncan R. The dawning era of polymer therapeutics. *Nat Rev Drug Discov* 2003;2:347–60.
- [5] Fox ME, Szoka FC, Frechet JM. Soluble polymer carriers for the treatment of cancer: the importance of molecular architecture. *Acc Chem Res* 2009;42:1141–51.
- [6] Deng C, Jiang Y, Cheng R, Meng F, Zhong Z. Biodegradable polymeric micelles for targeted and controlled anticancer drug delivery: promises, progress and prospects. *Nano Today* 2012;7:467–80.
- [7] Wang C, Wang Z, Zhang X. Amphiphilic building blocks for self-assembly: from amphiphiles to supra-amphiphiles. *Acc Chem Res* 2012;45:608–18.
- [8] Nicolas J, Mura S, Brambilla D, Mackiewicz N, Couvreur P. Design, functionalization strategies and biomedical applications of targeted biodegradable/biocompatible polymer-based nanocarriers for drug delivery. *Chem Soc Rev* 2013;42:1147–235.
- [9] Kazunori K, Glenn SK, Masayuki Y, Teruo O, Yasuhisa S. Block copolymer micelles as vehicles for drug delivery. *J Control Release* 1993;24:119–32.
- [10] Allen TM, Cullis PR. Drug delivery systems: entering the mainstream. *Science* 2004;303:1818–22.
- [11] Hu X, Liu S, Chen X, Mo G, Xie Z, Jing X. Biodegradable amphiphilic block copolymers bearing protected hydroxyl groups: synthesis and characterization. *Biomacromolecules* 2008;9:553–60.
- [12] Basarkar A, Singh J. Poly (lactide-co-glycolide)-polymethacrylate nanoparticles for intramuscular delivery of plasmid encoding interleukin-10 to prevent autoimmune diabetes in mice. *Pharm Res* 2009;26:72–81.
- [13] Sun Y, Yan X, Yuan T, Liang J, Fan Y, Gu Z, et al. Disassemblable micelles based on reduction-degradable amphiphilic graft copolymers for intracellular delivery of doxorubicin. *Biomaterials* 2010;31:7124–31.
- [14] Guo X, Shi C, Wang J, Di S, Zhou S. pH-triggered intracellular release from actively targeting polymer micelles. *Biomaterials* 2013;34:4544–54.
- [15] Rosen HB, Chang J, Wnek GE, Linhardt RJ, Langer R. Bioerodible polyanhydrides for controlled drug delivery. *Biomaterials* 1983;4:131–3.
- [16] Kumar N, Langer RS, Domb AJ. Polyanhydrides: an overview. *Adv Drug Deliv Rev* 2002;54:889–910.
- [17] Zhao A, Zhou S, Zhou Q, Chen T. Thermosensitive micelles from PEG-based ether-anhydride triblock copolymers. *Pharm Res* 2010;27:1627–43.
- [18] Chen T, Guo X, Liu X, Shi S, Wang J, Shi C, et al. A strategy in the design of micellar shape for cancer therapy. *Adv Healthcare Mater* 2012;1:214–24.
- [19] Griset AP, Walpole J, Liu R, Gaffey A, Colson YL, Grinstaff MW. Expansile nanoparticles: synthesis, characterization, and *in vivo* efficacy of an acid-responsive polymeric drug delivery system. *J Am Chem Soc* 2009;131:2469–71.
- [20] Wang J, Sun X, Mao W, Sun W, Tang J, Sui M, et al. Tumor redox heterogeneity-responsive prodrug nanocapsules for cancer chemotherapy. *Adv Mater* 2013;25:3670–6.
- [21] Yang Y, Wang J, Zhang X, Lu W, Zhang Q. A novel mixed micelle gel with thermo-sensitive property for the local delivery of docetaxel. *J Control Release* 2009;135:175–82.
- [22] Dai J, Lin S, Cheng D, Zou S, Shuai X. Interlayer-crosslinked micelle with partially hydrated core showing reduction and pH dual sensitivity for pin-pointed intracellular drug release. *Angew Chem Int Ed Engl* 2011;50:9404–8.
- [23] Yoon S, Kim WJ, Yoo HS. Dual-responsive breakdown of nanostructures with high doxorubicin payload for apoptotic anticancer therapy. *Small* 2013;9:284–93.
- [24] Liu J, Pang Y, Zhu Z, Wang D, Li C, Huang W, et al. Therapeutic nanocarriers with hydrogen peroxide-triggered drug release for cancer treatment. *Biomacromolecules* 2013;14:1627–36.
- [25] Cheng R, Feng F, Meng F, Deng C, Feijen J, Zhong Z. Glutathione-responsive nano-vehicles as a promising platform for targeted intracellular drug and gene delivery. *J Control Release* 2011;152:2–12.
- [26] Wei H, Zhuo R-X, Zhang X-Z. Design and development of polymeric micelles with cleavable links for intracellular drug delivery. *Prog Polym Sci* 2013;38:503–35.
- [27] Gilbert HF. In: Lester P, editor. Thiol/disulfide exchange equilibria and disulfide bond stability. *Methods Enzymol Academic Press*; 1995. pp. 8–28.
- [28] Shim MS, Kwon YJ. Stimuli-responsive polymers and nanomaterials for gene delivery and imaging applications. *Adv Drug Deliv Rev* 2012;64:1046–59.
- [29] Liu J, Pang Y, Chen J, Huang P, Huang W, Zhu X, et al. Hyperbranched polydisulfide as a self-assembling broad spectrum anticancer agent. *Biomaterials* 2012;33:7765–74.

- [30] Liu J, Huang W, Pang Y, Huang P, Zhu X, Zhou Y, et al. Molecular self-assembly of a homopolymer: an alternative to fabricate drug-delivery platforms for cancer therapy. *Angew Chem Int Ed Engl* 2011;50:9162–6.
- [31] Cheng Z, Al Zaki A, Hui JZ, Muzykantor VR, Tsourkas A. Multifunctional nanoparticles: cost versus benefit of adding targeting and imaging capabilities. *Science* 2012;338:903–10.
- [32] Meng F, Hennink WE, Zhong Z. Reduction-sensitive polymers and bio-conjugates for biomedical applications. *Biomaterials* 2009;30:2180–98.
- [33] Tang H, Murphy CJ, Zhang B, Shen Y, Van Kirk EA, Murdoch WJ, et al. Curcumin polymers as anticancer conjugates. *Biomaterials* 2010;31:7139–49.
- [34] Murphy CJ, Tang H, Van Kirk EA, Shen Y, Murdoch WJ. Reproductive effects of a pegylated curcumin. *Reprod Toxicol* 2012;34:120–4.
- [35] Yu H, Huang Q. Improving the oral bioavailability of curcumin using novel organogel-based nanoemulsions. *J Agric Food Chem* 2012;60:5373–9.
- [36] Akbari H, D'Emanuele A, Attwood D. Effect of geometry on the erosion characteristics of polyanhydride matrices. *Int J Pharm* 1998;160:83–9.
- [37] Hanes J, Chiba M, Langer R. Degradation of porous poly(anhydride-co-imide) microspheres and implications for controlled macromolecule delivery. *Biomaterials* 1998;19:163–72.
- [38] Wang YJ, Pan MH, Cheng AL, Lin LI, Ho YS, Hsieh CY, et al. Stability of curcumin in buffer solutions and characterization of its degradation products. *J Pharm Biomed Anal* 1997;15:1867–76.
- [39] Fleige E, Quadir MA, Haag R. Stimuli-responsive polymeric nanocarriers for the controlled transport of active compounds: concepts and applications. *Adv Drug Deliv Rev* 2012;64:866–84.
- [40] Hubbell JA. Enhancing drug function. *Science* 2003;300:595–6.
- [41] Sahoo SK, Ma W, Labhasetwar V. Efficacy of transferrin-conjugated paclitaxel-loaded nanoparticles in a murine model of prostate cancer. *Int J Cancer* 2004;112:335–40.
- [42] Yan Y, Johnston AP, Dodds SJ, Kamphuis MM, Ferguson C, Parton RG, et al. Uptake and intracellular fate of disulfide-bonded polymer hydrogel capsules for Doxorubicin delivery to colorectal cancer cells. *ACS Nano* 2010;4:2928–36.
- [43] Ravindran J, Prasad S, Aggarwal BB. Curcumin and cancer cells: how many ways can curry kill tumor cells selectively? *AAPS J* 2009;11:495–510.
- [44] Beevers CS, Li F, Liu L, Huang S. Curcumin inhibits the mammalian target of rapamycin-mediated signaling pathways in cancer cells. *Int J Cancer* 2006;119:757–64.
- [45] Song Z, Feng R, Sun M, Guo C, Gao Y, Li L, et al. Curcumin-loaded PLGA-PEG-PLGA triblock copolymeric micelles: preparation, pharmacokinetics and distribution in vivo. *J Colloid Interface Sci* 2011;354:116–23.
- [46] Smola M, Vandamme T, Sokolowski A. Nanocarriers as pulmonary drug delivery systems to treat and to diagnose respiratory and non respiratory diseases. *Int J Nanomed* 2008;3:1.
- [47] Maeda H, Wu J, Sawa T, Matsumura Y, Hori K. Tumor vascular permeability and the EPR effect in macromolecular therapeutics: a review. *J Control Release* 2000;65:271–84.
- [48] Lu J, Huang Y, Zhao W, Marquez RT, Meng X, Li J, et al. PEG-derivatized embelin as a nanomicellar carrier for delivery of paclitaxel to breast and prostate cancers. *Biomaterials* 2013;34:1591–600.
- [49] Wang B, He X, Zhang Z, Zhao Y, Feng W. Metabolism of nanomaterials in vivo: blood circulation and organ clearance. *Acc Chem Res* 2013;46:761–9.
- [50] Li L, Braiteh FS, Kurzrock R. Liposome-encapsulated curcumin: in vitro and in vivo effects on proliferation, apoptosis, signaling, and angiogenesis. *Cancer* 2005;104:1322–31.
- [51] Wang W, Cheng D, Gong F, Miao X, Shuai X. Design of multifunctional micelle for tumor-targeted intracellular drug release and fluorescent imaging. *Adv Mater* 2012;24:115–20.
- [52] Fan H, Hu QD, Xu FJ, Liang WQ, Tang GP, Yang WT. In vivo treatment of tumors using host-guest conjugated nanoparticles functionalized with doxorubicin and therapeutic gene pTRAIL. *Biomaterials* 2012;33:1428–36.